Received: 18 December 2017 | Revised: 4 August 2018 | Accepted: 1 October 2018

DOI: 10.1002/stc.2285

RESEARCH ARTICLE

WILEY

Evaluation of InSAR monitoring data for post-tunnelling settlement damage assessment

Giorgia Giardina[1] | Pietro Milillo[2] | Matthew J. DeJong[3] | Daniele Perissin[4] | Giovanni Milillo[5]

[1]Department of Architecture and Civil Engineering, University of Bath, Bath, UK

[2]NASA Jet Propulsion Laboratory, California Institute of Technology, Pasadena, California

[3]Department of Civil and Environmental Engineering, University of California, Berkeley, Berkeley, California

[4]Lyles School of Civil Engineering, Purdue University, West Lafayette, Indiana

[5]Italian Space Agency, Rome, Italy

Correspondence
Giorgia Giardina, Department of Architecture and Civil Engineering, University of Bath, Bath, UK.
Email: g.giardina@bath.ac.uk

Summary

The increasing demand for underground infrastructure should be supported by innovation in monitoring and damage assessment solutions to minimise damage to surface structures caused by ground settlements. This paper evaluates the use of multitemporal synthetic aperture radar interferometry (MT-InSAR) to calculate tunnelling-induced deformations of buildings. The paper introduces a step-by-step procedure to use InSAR displacements as an input to the structural damage assessment. After a comparison between traditional and InSAR monitoring data for the London area during the Crossrail excavation, the high resolution, high density InSAR-based displacements were used to evaluate the building deformations for a number of case studies. Results demonstrate the quality of information provided by InSAR data on soil-structure interaction mechanisms. Such information, essential to evaluate current damage assessment procedures, is typically only collected for relatively few buildings due to the cost of traditional monitoring. A comparison between damage indicators derived from greenfield assumptions and building displacements quantifies the practical benefit of the proposed step-by-step procedure. This work aims at filling the gap between the most recent advances in remote sensing and the civil engineering practice, defining the first step of an automated damage assessment procedure which can impact large scale underground projects in urban areas.

KEYWORDS

building damage, damage assessment, InSAR, multitemporal InSAR, settlements, soil–structure interaction, structural monitoring, tunnelling

1 | INTRODUCTION

Recent advances in tunnel technology, combined with population growth and rapid urbanisation, have led to an unprecedented development of urban tunnel constructions worldwide. In London alone, two major tunnelling projects (Thames Tideway Tunnel and Crossrail, at present the largest in Europe) are currently under construction, whereas another two (Crossrail 2, High Speed 2) are planned for the next decade, for a total expected investment of about £90bn.

A significant part of the total project costs relates to the management of the tunnelling impact on adjacent structures (e.g., £1bn out of £14.8bn for the Crossrail project). The interaction between the excavation and existing surface buildings can lead to structural damage, for example, unacceptable building deformations or cracking, and needs to be carefully

assessed in the preliminary stage of the project design. Health monitoring is then needed during the execution stage, typically only for the most vulnerable structures due to cost limitations, to determine the deformations that actually occur.

Assessment procedures[1-4] have been extensively employed in past and current projects (e.g., Jubilee Line Extension, Crossrail).[5,6] These procedures are based on simplifying assumptions regarding the structural behaviour; they neglect the influence of the soil–structure interaction on ground and building deformations and they tend to produce over-conservative results. Undesirable outcomes of their application can be the need to perform more advanced and time-consuming assessment (e.g., detailed finite element analyses) or to introduce potentially unnecessary mitigation measurements (e.g., compensation grouting).

On the other hand, recently proposed procedures,[7-10] which are based on a more accurate assessment of the soil-structure interaction, still encounter resistance in practice, mainly because of (a) uncertainties over the estimation of the structural information required as an input (e.g., building stiffness, existing building damage, building connectivity, foundation type and details),[11,12] (b) concerns over potentially inconsistent results between different procedures,[11,13] and (c) limited field data to evaluate procedures.[14] More details on current available damage assessment procedures will be given in Section 2.1.

The demand for high quality field data to develop and validate improved procedures has been previously highlighted.[13] In particular, the analysis of recent case studies[14] has emphasised the need to install several monitoring points on each structure to be able to accurately ascertain the building deformation caused by excavation. Buildings are particularly vulnerable to differential settlements, while absolute values of ground displacements do not provide a meaningful indication of potential damage. More specifically, damage assessment procedures begin with the evaluation of the settlement profile curvature affecting the structure (see Section 2.1), and therefore require the availability of three or more monitoring points along the length of the structure in the direction most relevant to the imposed deformation, that is, transverse to the tunnel axis. The importance of differential displacement measurements which are accurate and densely distributed over a vast territory makes the assessment of tunnelling-induced damage to buildings an ideal application for the recent advances of interferometric synthetic aperture radar (InSAR) techniques.

Synthetic aperture radar interferometry is a remote sensing technique for measuring surface deformations over time.[15] It provides high resolution, day-and-night and weather-independent images that can be used to monitor deformations over extensive areas. Although the potential of InSAR for monitoring of structures and infrastructure has been extensively proven,[16-25] only the recent availability of high resolution X-band (3-cm wavelength) spaceborne SAR Constellations such as COSMO-SkyMed[26] has theoretically enabled the direct use of InSAR monitoring data as an input for a quantitative assessment of structural damage; a main reason for this is the increase of coherent pixel density over urban areas by 320% and 550% with respect to RADARSAT-1 and ENVISAT C-band satellites (5.66-cm wavelength).[27]

This paper evaluates the practical use of InSAR monitoring data for the assessment of tunnelling-induced damage to buildings. In particular, it demonstrates how satellite-based displacement measurements can provide information on the soil-structure interaction mechanism. Such information is essential for the accurate evaluation of the building response to settlements and needed on vast geographic areas to validate current and new damage assessment procedures.[13] Notably, given the availability of past satellite images, this technique can also be applied retrospectively, to monitor the response of structures which were not included in the in situ monitoring plan. The current lack of extensive field measurements is a strong motivator for this work.

A description of the adopted methodology for the assessment of tunnelling-induced damage to buildings, and more specifically for the evaluation of soil–structure interaction, is given in Section 2.1. Section 2.2 presents the synthetic aperture radar multi-temporal interferometry (MT-InSAR) technique adopted for the satellite image processing. These sections highlight the complementarities in terms of required inputs and available outputs of the two techniques, both focused on the evaluation of differential displacements. Section 3.1 shows the InSAR monitored deformations for a zero displacement benchmark in the centre of London, quantifying the data mean and standard deviation for different levels of coherence, whereas in Section 3.2, the ground- and InSAR-based soil surface settlements for a transversal section of the Crossrail tunnel tracks are compared. The paper then exemplifies the quality of available InSAR-based measurements at the building level (Section 4.1) and addresses bias treatment (Section 4.2). Finally, the InSAR measurements are used to quantify the soil–structure interaction effect and assess building damage (Section 5). This enables an evaluation of the feasibility of InSAR-based monitoring data to assess tunnelling-induced damage to surface structures.

2 | METHODOLOGY

2.1 | Building damage assessment

The ground surface typically induced by tunnel excavation (Figure 1) can expose structures to damaging deformations. In particular, the tensile strains provoked by the bending and shear component of these deformations are detrimental for

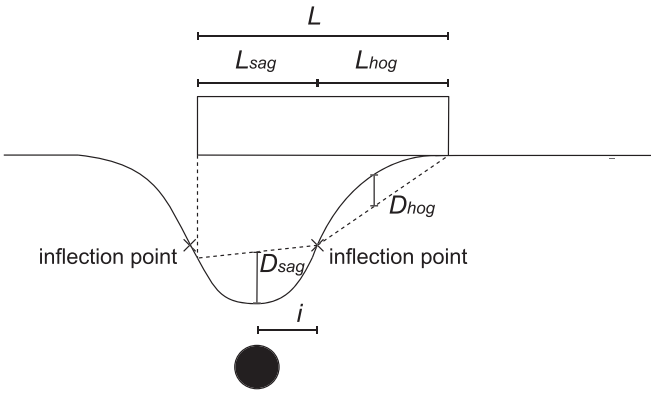

FIGURE 1 Tunnelling-induced settlement profile and deformation parameters for the sagging and hogging zone

quasi-brittle construction materials, such as unreinforced masonry. Current assessment procedures[3,4] therefore relate the deflection ratio (Δ/L in Figure 1) of the ground surface settlement profile, obtained by neglecting the influence of the structure on the settlement, with the maximum bending $\varepsilon_{b,\max}$ and diagonal $\varepsilon_{d,\max}$ strains arising in the structure:

$$\varepsilon_{b,\max} = \frac{\Delta/L}{\frac{1}{12}\frac{L}{t} + \frac{3}{2}\frac{I}{tLH}\frac{E}{G}}, \qquad \varepsilon_{d,\max} = \frac{\Delta/L}{1 + \frac{1}{18}\frac{HL^2}{I}\frac{G}{E}}, \tag{1}$$

where the bending over shear stiffness ratio E/G can be estimated and geometrical dimensions are known (building length L, height H and width B, also required to estimate the moment of inertia $I = \frac{1}{12}BH^3$). The distance between the assumed position of the building neutral axis n and the furthest fibre in tension is defined as t. Typically assumed values are $t = H/2$ in the sagging part of the settlement trough and $t = H$ in the hogging part of the profile.[1]

In this simplified method, the imposed deformation, quantified by Δ/L, is evaluated for greenfield conditions, that is, neglecting the building influence, generally through empirical–analytical expressions.[28-30] The resulting damage predictions tend to be conservative, because this estimation does not take into account soil-structure interaction. The interaction influence mainly consists of a reduction of the settlement trough curvature due to the building weight and stiffness, and hence depends on structural features such as building dimensions, presence of openings, building typology, and construction material.

The soil–structure interaction effect can be quantified by comparing the actual and greenfield deformation trough the modification factor $M_{\Delta/L}$ in the sagging and hogging part of the settlement profile[7]:

$$M_{(\Delta/L)_{sag}} = \frac{(\Delta/L)_{sag}}{(\Delta/L)_{gr,sag}}, \qquad M_{(\Delta/L)_{hog}} = \frac{(\Delta/L)_{hog}}{(\Delta/L)_{gr,hog}}, \tag{2}$$

where Δ/L is the actual building deflection ratio and $(\Delta/L)_{gr}$ is the greenfield deflection ratio. The indices *sag* and *hog* refer to the sagging and hogging zones, respectively (Figure 1).

Despite the potential economic advantage in terms of saved additional computational analyses and/or mitigation measures, these refined procedures are rarely adopted in practice, as stated previously. Centrifuge testing and numerical modelling have deepened understanding of the interaction mechanism[31-34] and have contributed to both the evaluation of current procedures and the proposal of new approaches.[13] However, an extensive amount of high quality field data would enable their rapid development, systematic validation, and practical implementation.

2.2 | Synthetic aperture radar interferometry

SAR (synthetic aperture radar) is a coherent active sensor operating in the microwave band; it exploits relative motion between antenna and target in order to obtain a finer spatial resolution in the flight direction (Azimuth), using the Doppler effect. In this way, it is possible to synthesise a kilometre-scale antenna with a several-metre real antenna (typically 10 m). In the direction transverse to the direction of flight (range), pulse modulation is used to increase resolution. The used microwave bands are almost free from atmospheric absorption and the radar signal to noise ratio (SNR) is high enough so that all weather, all time (day and night) imaging is possible.

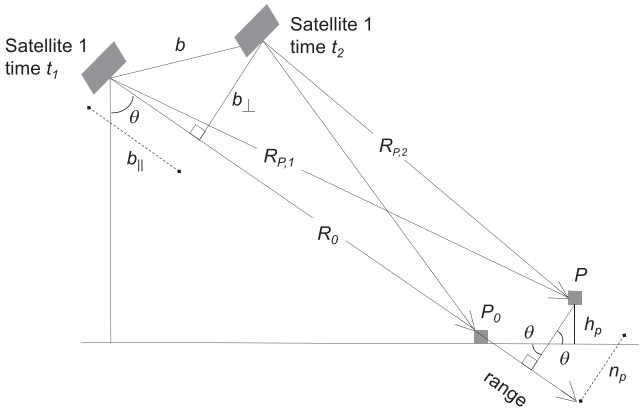

FIGURE 2 InSAR acquisition geometry. The same satellite acquires an image of the ground at different times (called temporal baseline) with a slightly different orbit position. The distance between the two orbits is called interferometric baseline (b). The InSAR is a technique capable of detecting relative height and differential displacements between the point P and a reference point P_0

Because SAR is a coherent sensor, it is possible to exploit phase information of the signal to estimate displacements occurring between two acquisitions separated in time. The method of retrieving relative displacements from two SAR images by exploiting the phase of the signal is called SAR Interferometry (InSAR) and consists of coherent cross-multiplication of two coherent signals and extraction of the phase component. If a satellite acquires two images at times t_1 and t_2, each acquisition is characterised by a certain distance from the previous pass called the interferometer baseline b (Figure 2). By varying the orbit of the same satellite and repeating the observation, the phase variation due to the different travel path of the signal can be determined. Assuming the far field approximation (i.e., the ratio between the baseline length b and the target-sensor distance is very small, of the order of 1/1000), the resulting phase difference is the following:

$$\phi_P = -\frac{4\pi}{\lambda}(R_{P,1} - R_{P,2}) = -\frac{4\pi}{\lambda}\Delta R_P = -\frac{4\pi b_\perp n_p}{\lambda R_0}, \tag{3}$$

where λ is the antenna wavelength, and R_0, $R_{P,1}$, and $R_{P,2}$, n_P and $b_\perp$ are indicated in Figure 2.

Because SAR is a side looking sensor, there will be a flat earth phase component due to the acquisition geometry. This component can be removed by knowing precisely the look angle θ. The phase component becomes the following:

$$\phi_P = -\frac{4\pi b_\perp h_P}{\lambda R_0 sin\theta}, \tag{4}$$

and thus, the height of point P can be written as follows:

$$h_P = -\frac{\lambda R_0 sin\theta}{4\pi b_\perp}\phi_p. \tag{5}$$

When $\phi = 2\pi$, the height of ambiguity, which is the height difference associated with the phase wrap, can be calculated. The height of ambiguity is an estimate of the interferometry sensitivity to topography. For b approaching zero, the SAR interferometer can not be used for topographic mapping. However, in this particular situation, assuming no temporal change in the atmospheric conditions, the interferometric phase depends only on the ground changes that have occurred in the time between the two acquisitions:

$$\phi_P = 2\pi\frac{\delta_p}{\lambda/2}. \tag{6}$$

This technique is called differential SAR interferometry (DInSAR) and is a powerful tool for detecting surface changes. From Equation 6, it follows that the differential interferometric sensitivity is inversely proportional to half of the wavelength, resulting in displacement accuracy of the order of millimetres.[19,35] Table 1 reports the comparison between theoretically achievable accuracies for ground- and InSAR-based monitoring systems.[35,36] It is not essential to have a zero baseline interferometer (although reducing the perpendicular baseline considerably improves the quality of the DInSAR product) in order to perform DInSAR.

TABLE 1 Theoretical accuracies for traditional and InSAR monitoring techniques[35,36]

Monitoring technique	Accuracy (mm)
Precise levelling	± 0.01
3D Prisms	± 1
InSAR	± 0.58–0.75

2.2.1 | Multitemporal technique MT-InSAR

Multitemporal analysis extended the DInSAR technique by combining several acquisitions, highlighting the relative displacement between each acquisition. In this paper, the MT-InSAR Technique described in Ferretti et al[37] was applied. This technique uses large baseline interferograms which are able to monitor only points maintaining the same scattering characteristics in time. Within this technique, the pixels are selected by studying their amplitude stability along the whole set of images. The permanent scatterers (PS) technique assumes a set of N+1 coregistered single-look complex SAR images. N single look differential interferograms with respect to a single master image were generated. The master image was chosen by maximising the expected coherence of the generated interferograms:

$$\gamma_{\text{temporal}}\gamma_{\text{spatial}}\gamma_{\text{doppler}} \approx \left[1 - f\left(\frac{T}{T_C}\right)\right]\left[1 - f\left(\frac{B_\perp}{B_{\perp C}}\right)\right]\left[1 - f\left(\frac{F_{DC}}{F_{DC}^C}\right)\right] \tag{7}$$

$$f(x) = \begin{cases} x & \text{for } x \leq 1 \\ 1 & \text{for } x > 1, \end{cases}$$

where $\gamma_{\text{temporal}}, \gamma_{\text{spatial}}$, and γ_{doppler} are the temporal, spatial and Doppler coherence, respectively, and T, T_C, $B_\perp$, $B_{\perp C}$, F_{DC}, and F_{DC}^C are the values for temporal, perpendicular, and doppler baseline, with the subscript C indicating the critical values beyond which the coherence drops to zero. A first rough identification of PS is performed by exploiting to the pixel amplitude stability. Choosing a pixel as a reference point, the interferometric phase ϕ for each pixel in the interferogram f can be defined as follows:

$$\phi = \phi_{\text{earth}} + \phi_{\text{topo}} + \phi_{\text{defo}} + \phi_{\text{atm}} + \phi_{\text{noise}}, \tag{8}$$

where the five terms capture the flat earth (due to the side looking SAR geometry), topographic, deformation, atmospheric and nuisance components, respectively.

If the constant velocity model[37] is valid, the atmospheric phase screen (APS) residues are due to atmospheric effects other than phase ramp and phase noise (mostly due to temporal and baseline decorrelation) and can be easily estimated. After estimating the APS, the target velocity and its height can be found by maximising the absolute value of the temporal coherence:

$$|\xi_{PS}| = \left| \frac{\sum_{f=1}^{K} e^{-j(\Delta\phi_{H,p}^f + \Delta\phi_{V,p}^f - \Delta\phi_p^f)}}{K} \right|, \tag{9}$$

where j is the complex unit, $\Delta\phi_{H,p}^f$ and $\Delta\phi_{V,p}^f$ are the phase terms that depend on the target height and the deformation velocity, respectively, and $\Delta\phi_p^f$ is the acquired interferometric phase compensated for flat terrain and APS. In some cases, the underlying assumption of linear displacement in Equation 9 is far from being true; thus, it is necessary to move from a deterministic model to a stochastic one, as proposed in Ferretti et al.[37] The PS candidates are unwrapped in space using the velocity and digital elevation model (DEM) error terms estimated with the linear velocity PS model. Once the data are unwrapped, the low pass component can be derived; this residual phase term is assumed as an estimation of the nonlinear motion contribution. The accuracy of the estimates can be derived by a regression analysis taking into account the irregularly sampled data (perpendicular baseline and temporal baseline in the case of the CSK constellation), as in Colesanti et al[38]:

$$\sigma_{\Delta h}^2 \approx \left(\frac{\lambda R \sin\theta}{4\pi}\right)^2 \frac{\sigma_\phi^2}{M\sigma_{Bp}^2}, \qquad \sigma_{\Delta v}^2 \approx \left(\frac{\lambda}{4\pi}\right)^2 \frac{\sigma_\phi^2}{M\sigma_{Bt}^2}, \tag{10}$$

where R is the target-sensor distance, θ is the incidence angle, λ is the sensor wavelength, σ^2_ϕ is the phase noise variance supposed independent of the acquisition, and σ^2_{Bp} and σ^2_{Bt} are the variance of the perpendicular and temporal baselines, respectively.

Extensive literature has been published focusing on structural monitoring of urban areas[39-43] and infrastructure, including dams,[22,23] railways,[44] and the effect of tunnelling.[17,45] MT-InSAR measurements provide coverage of ground displacements at high resolution and large spatial scales not reasonably accessible with in situ measurements such as leveling and GPS.

Different software tools are available for implementing multi-image InSAR techniques. In this work, SARPROZ[46] was used, and a nonlinear single master multitemporal time series analysis approach[37] was adopted. The analysed dataset includes 72 images acquired from April 2011 to December 2015 over the city of London, which were combined to produce time series of cumulative displacements.

Our data set consists of an interferometric stack of COSMO-SkyMed (CSK) Background Mission data. COSMO-SkyMed is a constellation of four X-band (3-cm wavelength) SAR satellites operated by the Italian Ministry of Defense and the Italian Space Agency (ASI). The CSK background mission project was developed by ASI, with the support of e-GEOS. The goal of the project is to provide interferometric mapping of urban areas with more than 100k inhabitants every 16 days in Stripmap mode (i.e., 3-m resolution) . The incidence angle of the satellite is 29° across the area of interest. Figure 3

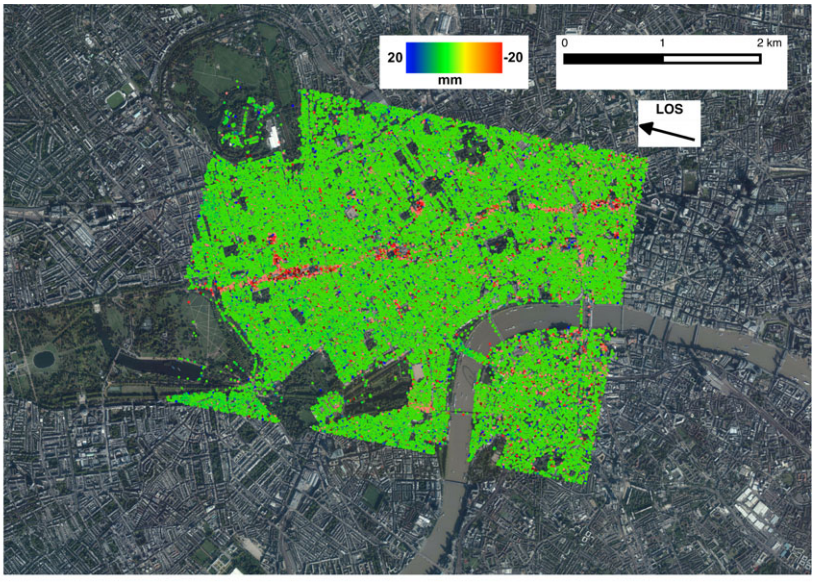

(a) Displacement map

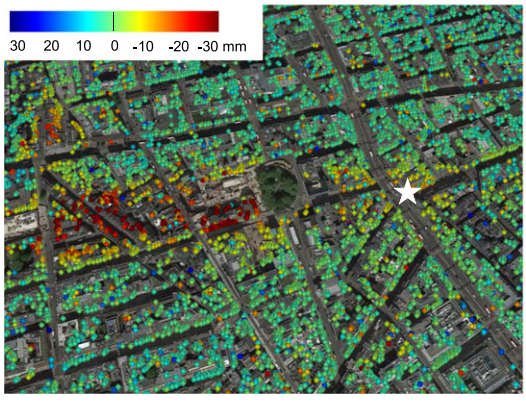

(b) Displacement map zoom-in. The star indicates the location of the example PS (Fig. 3c)

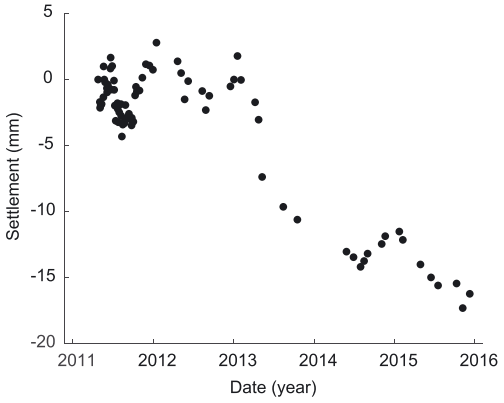

(c) Single PS time-series example

FIGURE 3 Cumulative displacements over London spanning April 2001–December 2015. Negative values indicate movements away from the satellite

shows a map of displacements that has occurred between April 2011 and December 2015; the ground settlement above the Crossrail twin tunnels is evident.

3 | GROUND DISPLACEMENTS

3.1 | Zero displacement evaluation

This work focuses on the evaluation of InSAR imagery to assess the impact of tunnelling excavations on buildings, specifically for the Crossrail project in London. Given the importance of data accuracy for a precise estimation of the building distortions, an example of MT-InSAR measurement quality is provided first. The measurements used as a reference are the cumulative displacements of a number of points located in Oxford Street, a major road in the centre of London (Figure 4). The portion of Oxford Street used for the evaluation runs almost parallel to the twin tunnel tracks at a distance of about 150 m from the nearest tunnel, thus outside the excavation area of influence. Because negligible ground displacements are expected in this area as a result of tunnelling, the location is considered an appropriate zero displacement reference.

Monitoring points at the ground surface level of Oxford Street were selected from the database (Figure 3a) according to their coordinates and estimated height. A measure of the data quality is given by the coherence, Equation 10. To give an indication of the suitability of InSAR data for structural applications, Figure 4 shows the increase in data accuracy when only data points above various threshold values of coherence c are considered. For $c > 0.9$, the measurements show a very limited scatter around the zero displacement, with a mean value μ of 3.3 mm and a standard deviation σ of 2.5 mm. A coherence greater than 0.9 is therefore recommended for structural risk assessment. All the data presented in the paper will follow this criterion.

3.2 | Tunnelling-induced displacement evaluation

After the evaluation of zero reference displacements, the InSAR monitoring performance was assessed through comparison with ground displacements acquired by precise levelling points (PLP) after the tunnel excavation. For the specific

(a) PS distribution

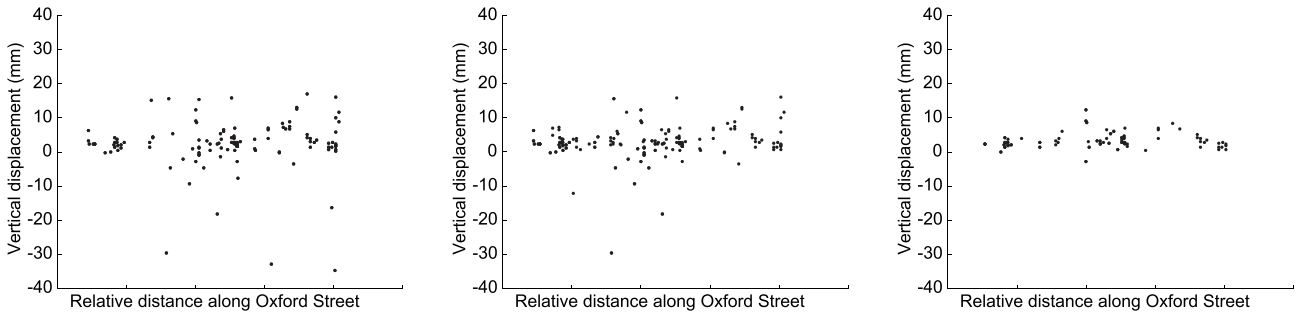

(b) $c > 0.7$, $\mu = 2.3$mm, $\sigma = 7.5$mm

(c) $c > 0.8$, $\mu = 2.4$mm, $\sigma = 5.5$mm

(d) $c > 0.9$, $\mu = 3.3$, $\sigma = 2.5$mm

FIGURE 4 Ground displacements, Oxford Street: (a) location of PSs and (b–d) refinement of results based on coherence c. For each case (b-d), the mean value for the settlement, μ, and the standard deviation, σ are reported

case of tunnelling-induced settlements, it is reasonable to assume that most of the displacement occurs vertically; hence, before analysing the InSAR time series, the MT-InSAR results were projected vertically according to the look angle.

Figure 5 shows the InSAR and PLP ground displacements measured along two adjacent sections in the direction transverse to the tunnel axis. Given their proximity (Figure 5a), the two sections are assumed to be affected by settlement profiles of equal shape and magnitude. Figure 5b shows that the InSAR measurements compare reasonably well with the PLP settlement trough. Note that the grey continuous curve represents the empirical-analytical estimation of the greenfield displacement S as a function of the horizontal distance x from the tunnel centreline:

$$S(x) = \sqrt{\frac{\pi}{2}} \frac{V_L D^2}{4i} e^{-\frac{x^2}{2i^2}}, \tag{11}$$

where V_L is the ratio of the volume of the surface settlement trough to the volume of the tunnel excavation and i is the horizontal distance between the tunnel centreline and the point of inflection of the settlement profile. V_L can be estimated through measurements at the soil surface where surface structures are not present, whereas the tunnel trough width i is typically calculated as $i = Kz$, where K is a parameter depending on the type of soil and excavation and z is the tunnel depth.[47] Based on average values observed along the Crossrail route, values of $V_L = 0.7\%$ and $K = 0.5$ were assumed in this work.[14]

The Gaussian curve[28] described by Equation 11 models the settlement trough generated by a single tunnel. To take into account the combined effect of the Crossrail twin tunnels, two Gaussian curves were superimposed; the three scenarios illustrated in Figure 6 were considered, depending on the distance between the tunnel axes.[6] The case study in Figure 5b corresponds to the scenario where the distance between the two tunnels is less than $2i$ (Figure 6a). Given the good match between monitored displacements and the combined greenfield settlement profile (more examples are reported in DeJong et al[14]), the Gaussian model was taken as a reference for greenfield displacements throughout the rest of this paper.

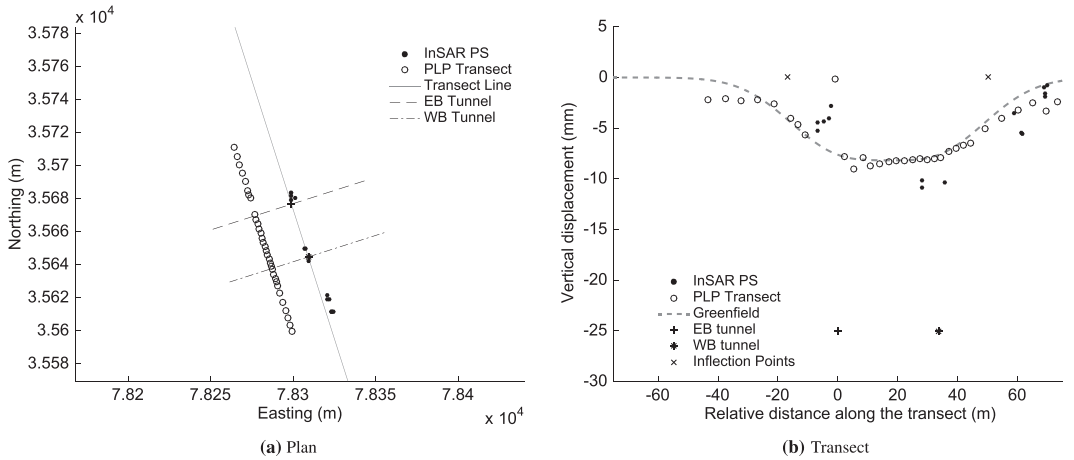

(a) Plan **(b)** Transect

FIGURE 5 Example of ground displacement data

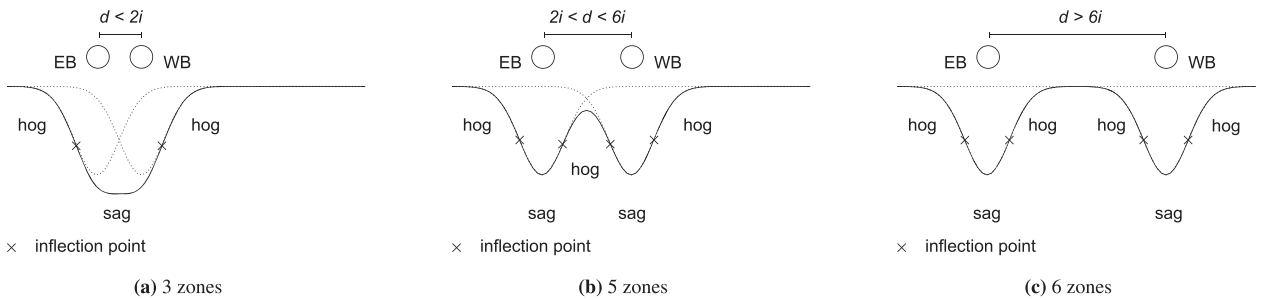

(a) 3 zones **(b)** 5 zones **(c)** 6 zones

FIGURE 6 General trough shapes for twin tunnels (after Crossrail[6]). The number of sagging (sag) and hogging (hog) zones depends on the distance d between the Eastbound (EB) and the Westbound (WB) tunnel and on the distance (i) between each inflection point and the corresponding tunnel

4 | BUILDING DISPLACEMENTS

4.1 | Data evaluation

The soil–structure interaction effect, which plays a key role in the actual building damage, can be quantified by comparing the ground and building settlements. This section illustrates the type of structural monitoring data made available by the MT-InSAR technique. The monitored structure is a nine-storey concrete building adjacent to the Crossrail tunnel excavation.

Figure 7a shows the location of InSAR monitoring points for the structure, which is located in between the two ground sections analysed in Section 3.2 (Figure 5a). Figure 7a highlights the high density of points available for a single building through MT-InSAR. This type of monitoring data fills the gap between the currently available datasets, can be obtained retrospectively as necessary, and provides the required inputs for accurate damage assessment.[14]

Figure 7b shows the InSAR monitored building settlements. The soil–structure interaction effect is emphasised by the comparison with the greenfield settlement profile fit to the displacements of the ground surface. The influence of the building is significant and mainly consists of two effects: (a) the reduction in curvature and related widening of the settlement trough and (b) the increase in the maximum displacement observed above the tunnel centrelines. Both mechanisms are compatible with the interaction between tunnelling and a relative stiff structure. In particular, regarding (a), similar effects of settlement profile flattening were observed in field monitoring,[48,49] experimental testing,[31,50,51] and numerical modelling,[7,9,32,52,53] and regarding (b), soil compaction and consequent larger displacements above the tunnel match recent centrifuge results[33,34] for building located in an asymmetric position with the tunnel and with one end of the building immediately above the tunnel axis. More examples of InSAR measurements for buildings are reported in Appendix A.

4.2 | Bias treatment

Given the differential nature of the InSAR measurements, there are some potential biases and errors that can be introduced in the time series due to the noise level and the satellite acquisition strategy. In this section, these biases are discussed, with specific focus on how to recognise potential unwrapping errors and ground reference point offsets.

4.2.1 | Phase unwrapping errors

As previously defined, an interferogram is an image formed by level curves indicating deformation changes. This information is only related to the last part of signal path and is wrapped by a modulus of 2π. From a mathematical point of view, we can define a 2π periodic function as follows:

$$\psi(t) = \phi(t) + 2\pi k \qquad k \in \mathbb{N}. \tag{12}$$

The phase unwrapping[54] consists in estimating ψ starting from ϕ. This is an ill posed problem because the wrapping operator is not invertible. Phase unwrapping errors can propagate in time series analysis introducing offsets of half sensor

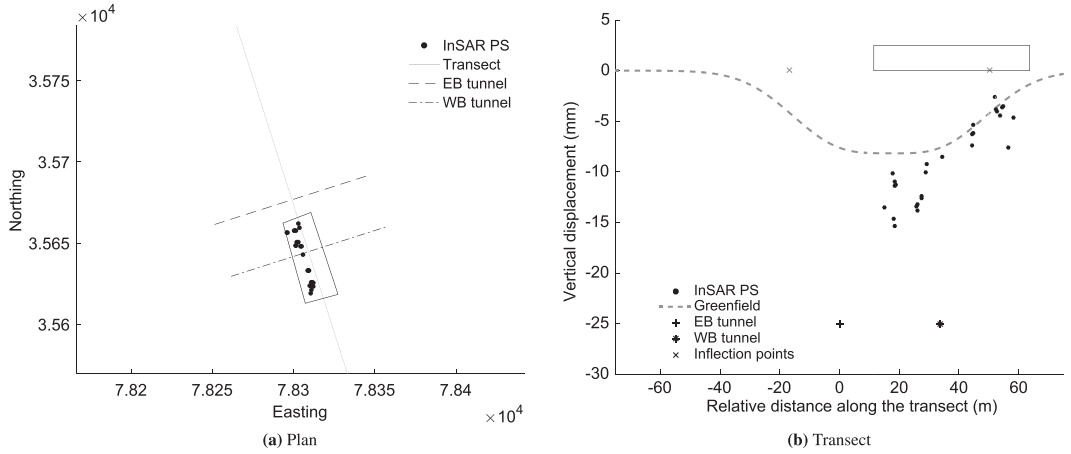

FIGURE 7 Example of building displacement data

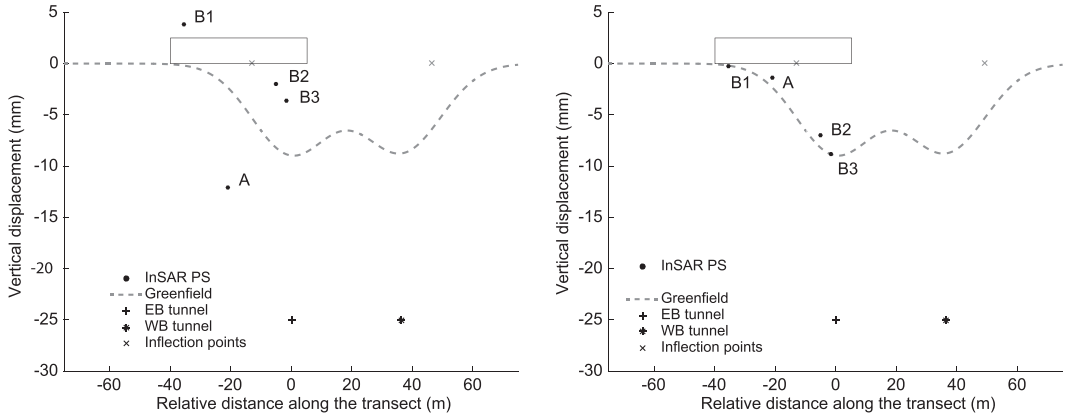

(a) Before correction **(b)** After correction

FIGURE 8 Comparison between raw data and monitoring results after phase unwrapping and shift correction

wavelength. A typical phase unwrapping error at X band (3-cm wavelength) is shown in Figure 8a, where point A is shifted by 1.5 cm. These kinds of error are easily detectable and can be corrected for points characterised by high temporal coherence values,[55,56] usually during the processing and post-processing step.[57] In this work, phase unwrapping errors have been automatically detected and corrected during the post-processing of displacements, as indicated by the shift of point A in Figure 8a,b.

4.2.2 | Reference point

As described in Section 2.2, MT-InSAR technique is a differential technique measuring the projection along the satellite line of sight (LOS) of the relative displacement of a point in the SAR image with respect to a reference point, assumed to be motionless or with known motion. Two main constraints apply to the reference point selection: (a) the point has to be characterised by high temporal coherence values (i.e., $c \geq 0.9$) within the area of interest and (b) the point should not be affected by a local displacement. In both cases, the time series of the reference point will be reflected in a signal common to all the time series.[58] This characteristic makes the identification of a wrong reference point easy because the mean value of the whole time series will be shifted from zero. Moreover, statistical analysis shows that atmospheric noise increases with the distance from the reference point, which affects the overall time series accuracy. For small area analyses (<10 km^2) as in our case, a standard deviation of the displacement values of 2–3 mm is reasonable.[58] For infrastructure analyses, a reference point as close as to the area of interest is hence recommended. In this work, any potential shift due to the reference point selection has been corrected by monitoring the difference between the displacement of the PS closest to the zero reference (e.g., point B1 in Figure 8a) and the Gaussian fitting curve. For each case, all the building displacements were shifted by the same amount (e.g., points B1, B2, and B3 in Figure 8a,b).

5 | SOIL–STRUCTURE INTERACTION

This section illustrates the procedural steps proposed for the quantification of soil–structure interaction, and therefore rapid means for retrospective building deformation assessment that can be applied to an extensive stock of structures in the tunnel influence region.

5.1 | Data fitting

According to current damage assessment procedures, the vulnerability of a building to subsidence can be determined from an assumed settlement profile and specific structural parameters affecting the building stiffness (Equation 1). In the absence of information on the actual building displacements, a greenfield settlement profile is typically applied. Given the possibility of InSAR measurements such as the ones displayed in Figure 7b, the actual vertical displacement profile of the building can be used, leading to a more realistic assessment of the strains induced in the building. To quantify the soil–structure interaction effect for the building analysed in Section 4.1, the monitored displacements were first fitted

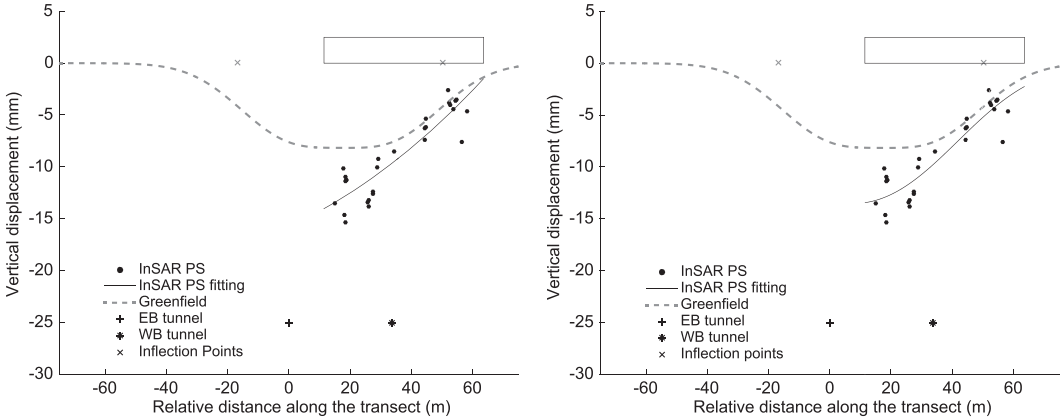

(a) Second order polynomial **(b)** Modified Gaussian

FIGURE 9 InSAR displacement data fitting

with an appropriate function. Then, the deflection ratio of this function was calculated over the building length. Finally, the building strains obtained by using the fitted deflection ratio were compared with the corresponding greenfield values.

Figure 9a shows that a second order polynomial provided a good fit of the data in this case. However, the goodness of fit at the building ends is highly dependent on the distribution of PS points along the building length. To address this, a modified Gaussian fitting function is instead proposed, based on the typical settlement trough cause by tunnelling.

The shape and magnitude of the Gaussian model for greenfield displacements depends on the trough width i and the volume loss V_L, which are defined based on physical characteristics of the problem (Equation 11). To increase the adaptability of this model, further degrees of freedom were introduced to produce modified Gaussian curves[29,30] based on experimental data in greenfield conditions. In this study, the concept of a modified Gaussian formulation was applied to fit soil–structure monitoring data. To take into account the typically observed effects of larger maximum settlements and wider profiles, the values of i and V_L were considered as variables. Furthermore, the position of the maximum displacement was not constrained to the tunnel centreline.[13] Three new coefficient α, β, and γ were therefore introduced:

$$x_m = \alpha + x, \qquad V_{Lm} = \beta V_L, \qquad i_m = \gamma i, \tag{13}$$

where i_m, V_{Lm}, and x_m are the modified trough width, volume loss, and horizontal coordinate, respectively. The superimposition illustrated in Figure 6 was applied to account for the twin tunnel effect.

Figure 9 shows an example of the fit provided by the modified Gaussian curve. More examples of fitted monitored displacements for buildings affected by the Crossrail tunnels are reported in Appendix A, including values of α, β, and γ for the analysed cases. The fitting function assumption will certainly affect the following damage assessment results. Where PS points are available over the entire length of the building, either fitting function considered was observed to provide similar results. However, where PS point data is less extensive, the modified Guassian fitting function provides much more realistic, and generally more conservative, results.

5.2 | Damage assessment

The deflection ratios obtained from the modified Gaussian curve fitting of the building data were used to calculate the total tensile strains, according to Equation 1. Note that based on the assumption that most of the deformations occur vertically, only the projected vertical displacements were used for the tensile strain assessment. This choice is supported by field[3,49,59] and centrifuge[31,33] observations, which confirm that relatively small horizontal strains are typically transferred to the building, and therefore the majority of the time they can be neglected in the assessment.

Figures 10a and 11a compare the building tensile strains based on the monitored deformations with the corresponding greenfield predictions, for all the analysed cases (Appendix A). The difference between building and greenfield values gives a measure of the effect of the building on the settlement profile. As expected, the assessment based on greenfield deformations is conservative for the vast majority of cases.

For the cases (e) and (l) (Figures 10a and A1e,l), the data fitting results in deflection ratios slightly larger than the greenfield equivalents. Overall, the comparison between Figures 10a and A1 indicate a reasonable interpretation of the

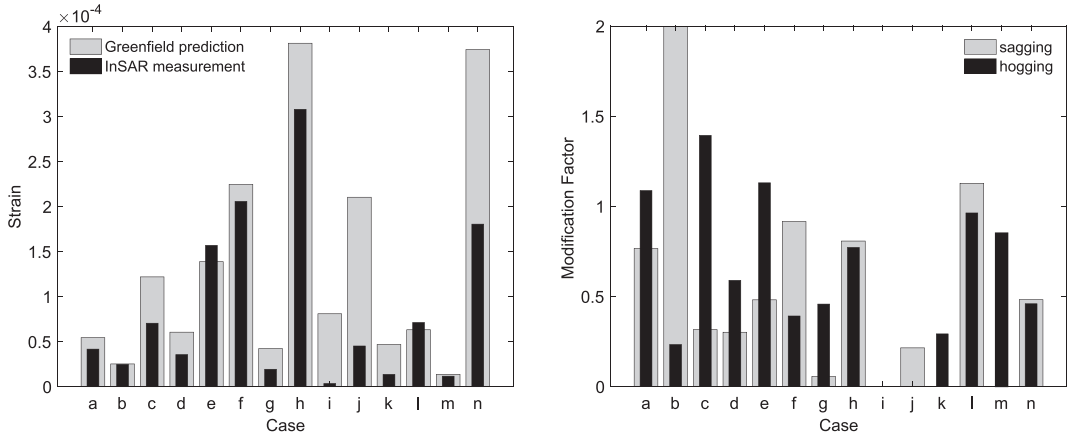

(a) Maximum strains (Eq. 1) **(b)** Modification factors (Eq. 2)

FIGURE 10 Damage indicators derived by InSAR monitored displacements for the buildings analysed in this study

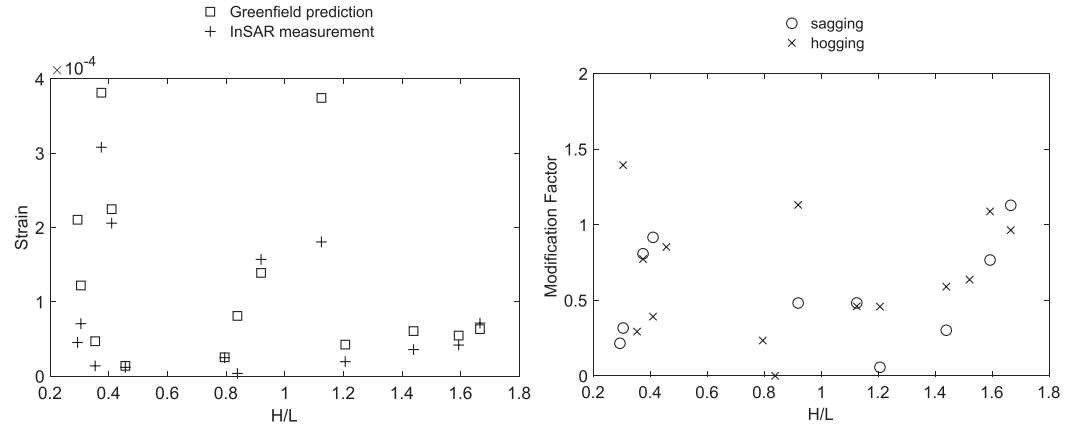

(a) Maximum strains (Eq. 1) **(b)** Modification factors (Eq. 2)

FIGURE 11 Damage indicators as a function of the H/L aspect ratio

building response: Depending on their dimension, weight, stiffness, and position, the structures tend to flatten and widen the settlement trough. Furthermore, consistently with recent centrifuge results,[31,33] reduced maximum settlements are observed for buildings spanning across the entire sagging zone of the settlement trough, whereas larger settlements are observed near the tunnel centreline for buildings located eccentrically to the tunnel.

The potential of the presented approach for the use of InSAR monitoring data as input for damage assessment procedures is further highlighted in Figures 10b and 11b. Modification factors, as defined in Equation 2, were derived for the sagging and hogging deformation mode of each building. Values smaller than one indicate that the presence of the building reduced the curvature of the settlement profile, leading to smaller building deformations compared with the greenfield predictions. Among the cases where the modification factors are much greater than 1, the analysis of the corresponding profiles in Figure A1 reveals that the largest $M_{\Delta/L}$ can be connected to a deformation mode affecting only a small portion of the structure. For example, the sagging modification factor of case (b) corresponds to a deflection ratio which is largely dependent on the very small building portion in sagging. This component is clearly not representative of the general building deformation. Similar results were found for centrifuge testing.[13] As a general guideline, modification factors should only be considered as a measure of the soil–structure interaction for the governing structural deformation mode.

In general, the results in Figures 10, 11, and A1 provide valuable data which can be retrospectively analysed. It should be noted that the reliability and accuracy of the resulting building deformation is clearly dependent on the number of PS points that can be obtained on a given building, and the coherence of those points. For example, Figure A1h represents a case were relatively few high-coherence PS points could be obtained. In this case, the building deformation is clearly less reliable.

6 | CONCLUSIONS

This work evaluates the use of InSAR monitoring data for the assessment of tunnelling-induced damage to surface structures. From the analysis of the COSMO-SkyMed dataset acquired over the London basin during the Crossrail excavation, the following conclusions can be drawn:

- The availability of high resolution and spatially dense MT-InSAR measurements of differential settlements makes this technique compatible with the requirements of damage assessment procedures, because it can provide a valuable estimation of the tunnelling-induced settlement profile.
- More specifically, the analysis of the mean and standard deviation for a benchmark dataset suggests that InSAR data with a coherence greater than 0.9 can provide accurate enough data to make useful conclusions regarding structural deformations. Further improving the accuracy of displacement data would enable more civil engineering applications, and increase confidence in results.
- The comparison between precise levelling points and permanent scatters showed that the InSAR-based measurements can capture both the shape and the magnitude of the typical settlement trough generated by a tunnel excavation.
- The InSAR building displacement data, fitted with a modified Gaussian model, provides a means to estimate the actual building settlement profile resulting from the soil–structure interaction. The availability of InSAR data for extensive areas, which can be obtained retrospectively, therefore offers the opportunity to obtain unprecedented insight, both in quantitative and qualitative terms, into the soil–structure interaction mechanism.
- The proposed step by step procedure gives practical guidelines for how to use InSAR data to conduct a post-tunnelling damage assessment based on actual building deformations. This procedure satisfies the demand for extensive, and relatively inexpensive, field data that is often unaffordable for urban excavation projects; notably, it also can provide data for past projects.

In summary, the procedure has the potential of (a) providing quasi-real time monitoring over large urban areas for automated early warning systems and (b) enabling rapid development and extensive validation of improved procedures for the structural damage assessment.

ACKNOWLEDGEMENTS

Original COSMO-SkyMed product ASI Agenzia Spaziale Italiana (2011-2016). Part of the research was carried out at the Jet Propulsion Laboratory, California Institute of Technology, under a contract with the National Aeronautics and Space Administration. The authors wish to thank Deborah Lazarus and David Ashworth for providing the leveling data included in Figure 5.

DATA ACCESS

The research materials supporting this publication can be accessed at https://doi.org/10.15125/BATH-00531.

ORCID

Giorgia Giardina http://orcid.org/0000-0002-5996-5830

REFERENCES

1. Burland JB, Wroth CP. Settlement of buildings and associated damage. In: Proceedings of Conference on Settlement of Structures. Cambridge: Pentech Press; 1974:611-654.
2. Boscardin MD, Cording EJ. Building response to excavation-induced settlement. *J Geotech Eng*. 1989;115(1):1-21.
3. Burland JB, Mair R, Standing RN. Ground performance and building response due to tunnelling. In: Jardine RJ, Potts DM, Higgins KG, eds. *Conference on Advances in Geotechnical Engineering*, London, Vol. 1: Institution of Civil Engineers; 2004:291-342.
4. Mair R, Taylor RN, Burland JB. Prediction of ground movements and assessment of risk of building damage due to bored tunnelling. In: Mair RJ, Taylor RN, eds. *Geotechnical Aspects of Underground Construction in Soft Ground. Proceedings of the International Symposium*. Rotterdam: Balkema; 1996:713-718.
5. Burland JB, Standing JR, Jardine FM. Building Response to Tunnelling: Case Studies from Construction of the Jubilee Line Extension, London In:Burland JB, R StandingJ, M JardineF, eds. *CIRIA Special Publication Series*. London: Thomas Telford; 2001.
6. Crossrail. Phase 2 generic building damage assessment report – Drive X running tunnels; 2011.

7. Potts DM, Addenbrooke TI. A structure's influence on tunnelling-induced ground movements. *Proc Inst Civ Eng Geotech Eng*. 1997;125(2):109-125.
8. Son M, Cording EJ. Estimation of building damage due to excavation-induced ground movements. *J Geotech Geoenviron Eng*. 2005;131(2):162-177.
9. Franzius JN, Potts DM, Burland JB. The response of surface structures to tunnel construction. *Proc Inst Civ Eng Geotech Eng*. 2006;159(1):3-17.
10. Goh KH, Mair R. The response of buildings to movements induced by deep excavations. *Geotech Eng J SEAGS and AGSSEA*. 2011;42(3):903-910.
11. Giardina G, DeJong MJ, Chalmers B, Ormond B, Mair RJ. A comparison of current analytical methods for predicting soil-structure interaction due to tunnelling. *Tunn Undergr Space Technol*. 2018;79:319-335.
12. Haji TK, Marshall A, Tizani W. A cantilever approach to estimate bending stiffness of buildings affected by tunnelling. *Tunn Undergr Space Technol*. 2018;71(Supplement C):47-61.
13. Ritter S. Tunnel-soil-structure interaction. *Ph.D. Thesis*: University of Cambridge; 2017.
14. DeJong MJ, Giardina G, Chalmers B, Lazarus D, Ashworth D, Mair RJ. The impact of tunnelling on loadbearing masonry buildings on shallow foundations (in review); 2018.
15. Rosen PA, Hensley S, Joughin IR, et al. Synthetic aperture radar interferometry. *Proc IEEE*. 2000;88(3):333-382.
16. Strozzi T, Delaloye R, Poffet D, Hansmann J, Loew S. Surface subsidence and uplift above a headrace tunnel in metamorphic basement rocks of the Swiss Alps as detected by satellite SAR interferometry. *Remote Sens Environ*. 2011;115(6):1353-1360.
17. Perissin D, Wang Z, Lin H. Shanghai subway tunnels and highways monitoring through Cosmo-SkyMed Persistent Scatterers. *ISPRS J Photogramm Remote Sens*. 2012;73(Supplement C):58-67.
18. Fornaro G, Reale D, Verde S. Bridge thermal dilation monitoring with millimeter sensitivity via multidimensional SAR Imaging. *IEEE Geosci Remote Sens Lett*. 2013;10(4):677-681.
19. Di Martire D, Iglesias R, Monells D, et al. Comparison between differential SAR interferometry and ground measurements data in the displacement monitoring of the earth-dam of Conza della Campania (Italy). *Remote Sens Environ*. 2014;148(Supplement C):58-69.
20. Lazecky M, Perissin D, Bakon M, de Sousa JM, Hlavacova I, Real N. Potential of satellite InSAR techniques for monitoring of bridge deformations. In: 2015 Joint Urban Remote Sensing Event (JURSE), Lausanne; 2015:1-4.
21. Cerchiello V, Tessari G, Velterop E, Riccard P, Defilippi M, Pasquali P. Risk of building damage by modeling interferometric time series. In: 2016 IEEE International Geoscience and Remote Sensing Symposium (IGARSS), Beijing; 2016:7334-7337.
22. Milillo P, Bürgmann R, Lundgren P, et al. Space geodetic monitoring of engineered structures: the ongoing destabilization of the Mosul dam, Iraq. *Sci Rep*. 2016;6:37408.
23. Milillo P, Perissin D, Salzer JT, Lundgren P, Lacava G, Milillo G, Serio C. Monitoring dam structural health from space: insights from novel InSAR techniques and multi-parametric modeling applied to the Pertusillo dam Basilicata, Italy. *Int J Appl Earth Obs Geoinf*. 2016;52(Supplement C):221-229.
24. Chang L, Dollevoet RPBJ, Hanssen RF. Nationwide railway monitoring using satellite SAR interferometry. *IEEE J Sel Top Appl Earth Observations Remote Sens*. 2017;10(2):596-604.
25. Bejarano-Urrego LE, Verstrynge E, Van Balen K, Wuyts V, Declercq PY. Settlement-induced damage monitoring of a historical building located in a coal mining area using PS-InSAR. In: Workshop on Civil Structural Health Monitoring. Queen's University; 2016; Belfast.
26. Milillo P, Riel B, Minchew B, Yun SH, Simons M, Lundgren P. On the synergistic use of SAR constellations's data exploitation for earth science and natural hazard response. *IEEE J Sel Top Appl Earth Observations Remote Sens*. 2016;9(3):1095-1100.
27. Bonano M, Manunta M, Pepe A, Paglia L, Lanari R. From previous C-band to new X-band SAR systems: assessment of the DInSAR mapping Improvement for deformation time-series retrieval in urban areas. *IEEE Trans Geosci Remote Sens*. 2013;51(4):1973-1984.
28. Peck RB. Deep excavations and tunneling in soft ground. In: Proceedings of the 7th International Conference on Soil Mechanics and Foundation Engineering; 1969; Mexico City. 225-290.
29. Vorster T, Klar A, Soga K, Mair RJ. Estimating the effects of tunneling on existing pipelines. *J Geotech Geoenviron Eng*. 2005;131(11):1399-1410.
30. Marshall A, Farrell R, Klar A, Mair R. Tunnels in sands: the effect of size, depth and volume loss on greenfield displacements. *Géotechnique*. 2012;62(5):385.
31. Farrell RP. Tunnelling in sands and the response of buildings. *Ph.D. Thesis*: University of Cambridge; 2010.
32. Giardina G, DeJong MJ, Mair RJ. Interaction between surface structures and tunnelling in sand: centrifuge and computational modelling. *Tunn Undergr Space Technol*. 2015;50:465-478.
33. Ritter S, DeJong MJ, Giardina G, Mair RJ. Influence of building characteristics on tunnelling-induced ground movements. *Geotechnique*. 2017;67(10):926-937.
34. Ritter S, Giardina G, DeJong MJ, Mair RJ. Centrifuge modelling of building response to tunnel excavation. *Int J Phys Modell Geotechnics*. 2017;18(3):146-161.
35. Ferretti A, Savio G, Barzaghi R, et al. Submillimeter accuracy of InSAR time series: experimental validation. *IEEE Trans Geosci Remote Sens*. 2007;45(5):1142-1153.
36. Gonzáles-Martí JG, Sánchez J, Symoniou D, Brzeski J. The thinner pen paradox. *Crossrail learning legacy report*. London, UK: Crossrail Ltd.; 2017.

37. Ferretti A, Prati C, Rocca F. Permanent scatterers in SAR interferometry. *IEEE Trans Geosci Remote Sens*. 2001;39(1):8-20.
38. Colesanti C, Ferretti A, Novali F, Prati C, Rocca F. SAR monitoring of progressive and seasonal ground deformation using the permanent scatterers technique. *IEEE Trans Geosci Remote Sens*. 2003;41(7):1685-1701.
39. Perissin D, Wang T. Time-series InSAR applications over urban areas in China. *IEEE J Sel Top Appl Earth Observations Remote Sens*. 2011;4(1):92-100.
40. Tapete D, Fanti R, Cecchi R, Petrangeli P, Casagli N. Satellite radar interferometry for monitoring and early-stage warning of structural instability in archaeological sites. *J Geophys Eng*. 2012;9(4):S10-S25.
41. Cigna F, Lasaponara R, Masini N, Milillo P, Tapete D. Persistent scatterer interferometry processing of COSMO-SkyMed StripMap HIMAGE time series to depict deformation of the historic centre of Rome, Italy. *Remote Sens*. 2014;6(12):12593-12618.
42. Pratesi F, Tapete D, Terenzi G, Del Ventisette C, Moretti S. Rating health and stability of engineering structures via classification indexes of InSAR Persistent Scatterers. *Int J Appl Earth Obs Geoinf*. 2015;40(Supplement C):81-90.
43. Milillo P, Tapete D, Cigna F, et al. Structural health monitoring of engineered structures using a space-borne synthetic aperture radar multi-temporal approach: from cultural heritage sites to war zones. In: SPIE Proceedings : SAR Image Analysis, Modeling, and Techniques XVI. SPIE; 2016; Edinburgh, UK:100030N.
44. Qin X, Liao M, Zhang L, Yang M. Structural health and stability assessment of high-speed railways via thermal dilation mapping with Time-Series InSAR Analysis. *IEEE J Sel Top Appl Earth Observations Remote Sens*. 2017;10(6):2999-3010.
45. Gonzáles-Martí JG, Nevard S, Sánchez J. The use of InSAR (Interferometric Synthetic Aperture Radar) to complement control of construction and protect third party assets. Crossrail Learning Legacy Report, London, UK, Crossrail Ltd.; 2017.
46. Perissin Daniele, Wang Zhiying, Wang Teng. The SARPROZ InSAR tool for urban subsidence/manmade structure stability monitoring in China. In: Proc. of ISRSE 2010; 2011; Sydney, Australia. 10-15.
47. O'Reilly MP, New BM. Settlement above tunnels in the United Kingdom—their magnitude and prediction. In: Tunnelling 82. Proceedings of the 3rd International Symposium. Institution of Mining and Metallurgy; 1982; London. 173-181.
48. Frischmann WW, Hellings JE, Snowden C. Protection of the Mansion House against damage caused by ground movements due to the Docklands Light Railway Extension. In: Proceedings of the Institution of Civil Engineers: Geotechnical Engineering, Vol. 107; 1994:65-76.
49. Burland JB, Standing JR, Jardine FM. *Building Response to Tunnelling: Case Studies from Construction of the Jubilee Line Extension*. London, UK: Ciria and Thomas Telford; 2001.
50. Taylor R, Yip D. Centrifuge modelling on the effect of a structure on tunnelling-induced ground movements. In: Response of Buildings to Excavation-induced Ground Movements Conference. CIRIA; 2001; London, UK. 601-611.
51. Caporaletti P, Burghignoli A, Taylor R. Centrifuge study of tunnel movements and their interaction with structures. In: Bakker K J, Bezuijen A, Broere W, Kwas E A, eds. *Geotechnical Aspects of Underground Construction in Soft Ground: Proceedings of the 5th International Symposium TC28, Amsterdam, the Netherlands*. London, UK: CRC Press; 2005:99-106.
52. Liu G, Houlsby GT, Augarde CE. 2-dimensional analysis of settlement damage to masonry buildings caused by tunnelling. *Struct Eng*. 2000;79(1):19-25English.
53. Amorosi A, Boldini D, De Felice G, Malena M, Sebastianelli M. Tunnelling-induced deformation and damage on historical masonry structures. *Géotechnique*. 2014;64(2):118-130.
54. Goldstein RM, Zebker HA, Werner CL. Satellite radar interferometry: two-dimensional phase unwrapping. *Radio sci*. 1988;23(4):713-720.
55. Pepe A, Lanari R. On the extension of the minimum cost flow algorithm for phase unwrapping of multitemporal differential SAR interferograms. *IEEE Trans Geosci Remote Sens*. 2006;44(9):2374-2383.
56. Shanker AP, Zebker H. Edgelist phase unwrapping algorithm for time series InSAR analysis. *JOSA A*. 2010;27(3):605-612.
57. Pritt MD. Automatic correction of phase unwrapping errors. US Patent 6,150,973; 2000.
58. Ferretti A. *Satellite InSAR Data: Reservoir Monitoring from Space*. The Netherlands: EAGE Publications; 2014.
59. Mair RJ. Tunnelling and deep excavations: ground movements and their effects. In: Proceedings of the 15th European Conference on Soil Mechanics and Geotechnical Engineering - Geotechnics of Hard Soils - Weak Rocks (Part 4). Amsterdam: IOS Press; 2013:39-70.

How to cite this article: Giardina G, Milillo P, DeJong MJ, Perissin D, Milillo G. Evaluation of InSAR monitoring data for post-tunnelling settlement damage assessment. *Struct Control Health Monit*. 2019;26:e2285. https://doi.org/10.1002/stc.2285

APPENDIX A: ANALYSED CROSSRAIL CASES

This section reports the PS distribution and monitored displacements for 14 building adjacent to the tunnel track. The selected buildings are located in areas where the ground movements were not influenced by station box excavations. For each building, the plan indicates the position of the structure with respect to the twin tunnel excavation.

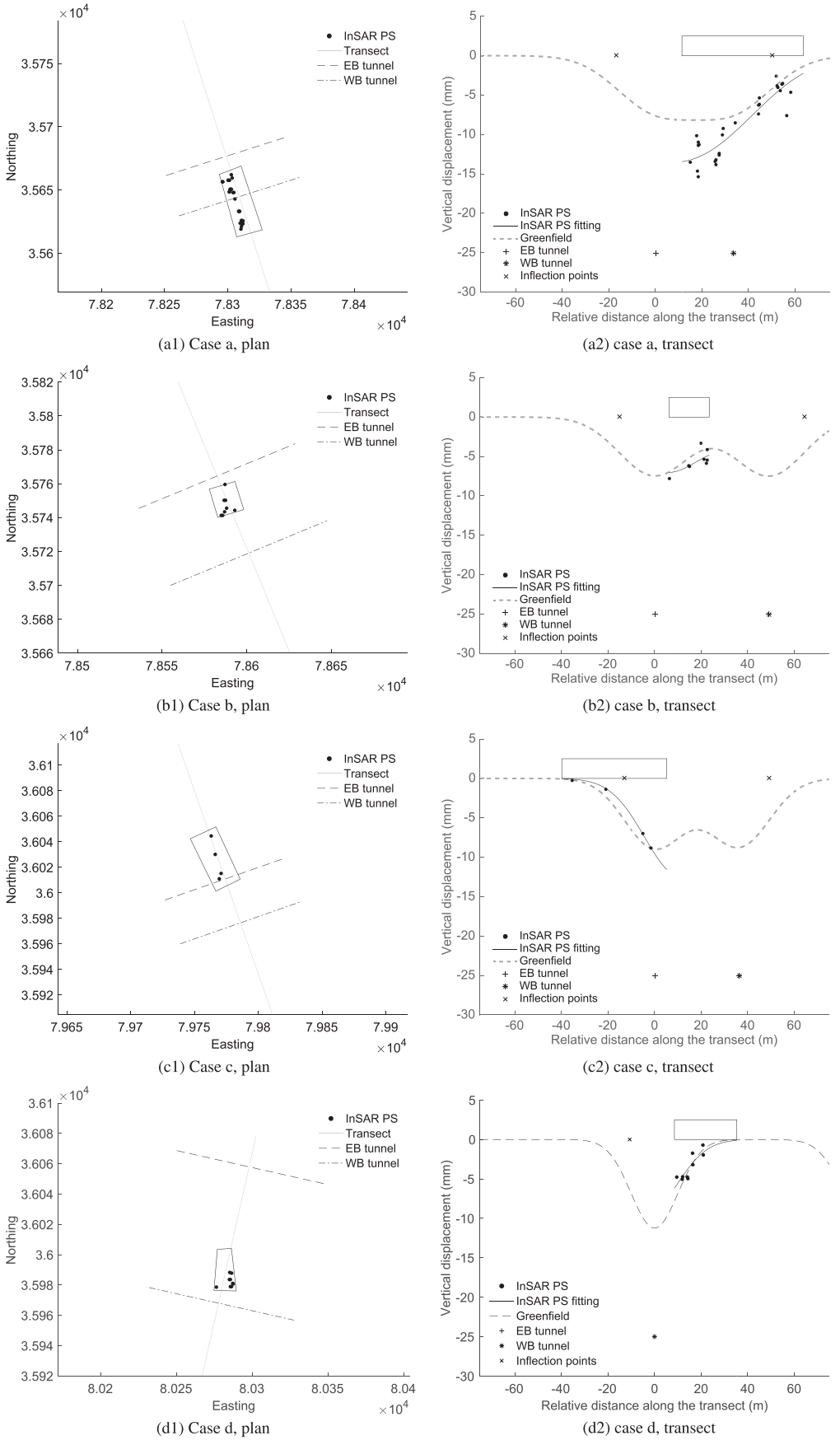

(a1) Case a, plan

(a2) case a, transect

(b1) Case b, plan

(b2) case b, transect

(c1) Case c, plan

(c2) case c, transect

(d1) Case d, plan

(d2) case d, transect

FIGURE A1 InSAR displacement data for the buildings analysed in this study

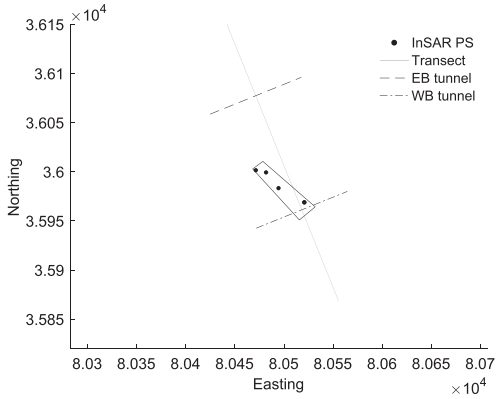

(e1) Case e, plan

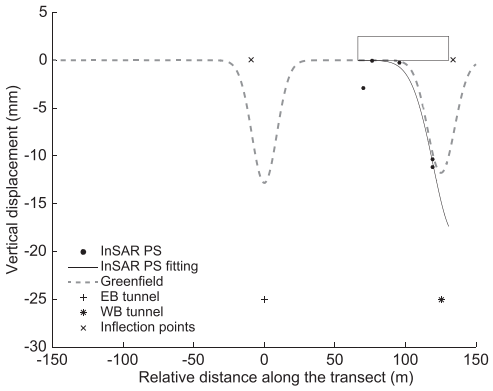

(e2) case e, transect

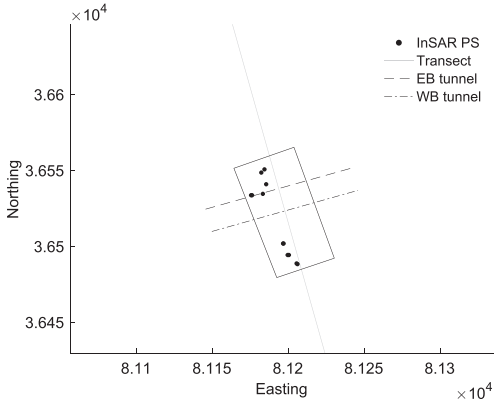

(f1) Case f, plan

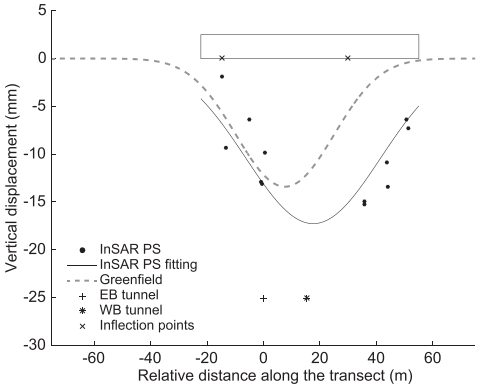

(f2) case f, transect

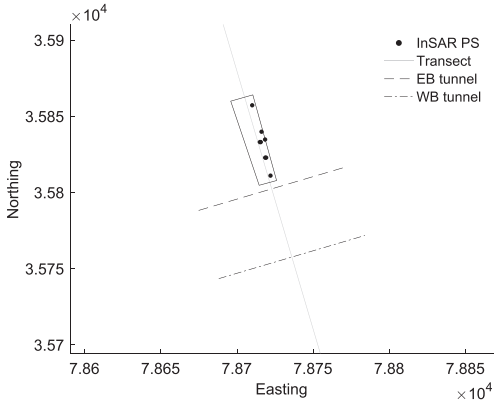

(g1) Case g, plan

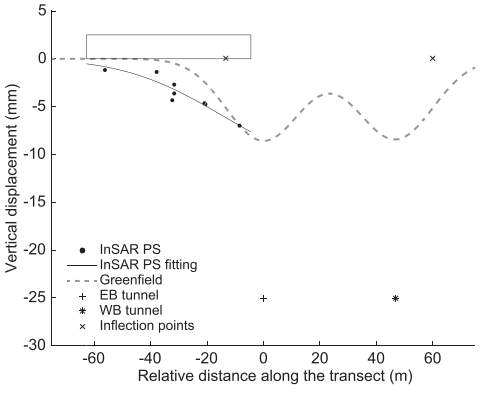

(g2) case g, transect

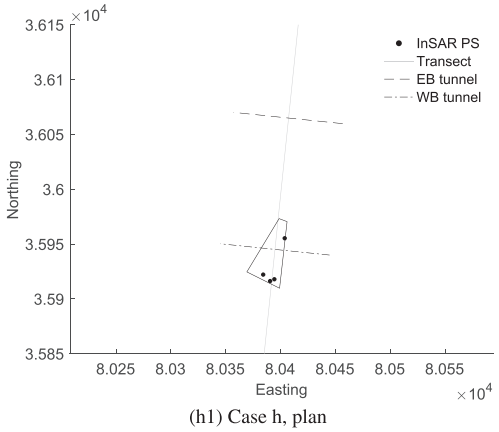

(h1) Case h, plan

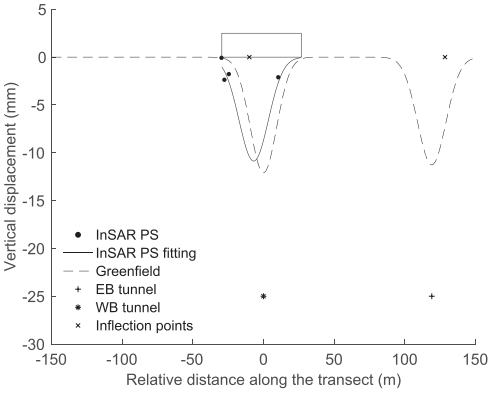

(h2) case h, transect

FIGURE A1 Continued

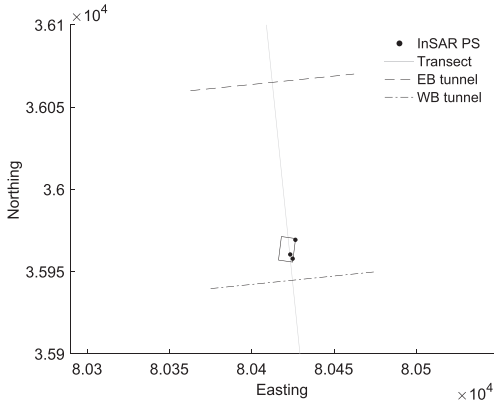

(i1) Case i, plan

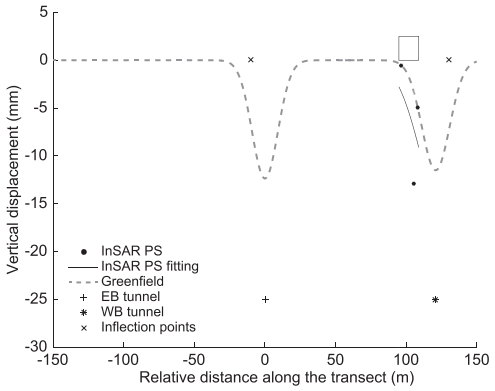

(i2) case i, transect

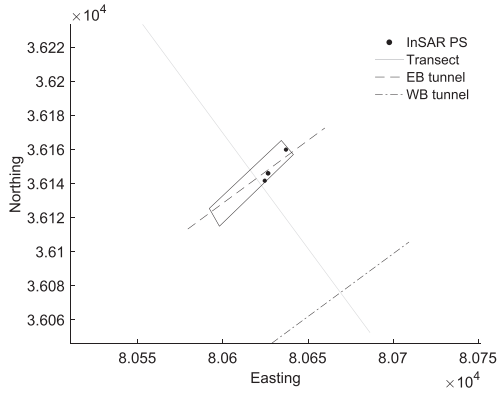

(j1) Case j, plan

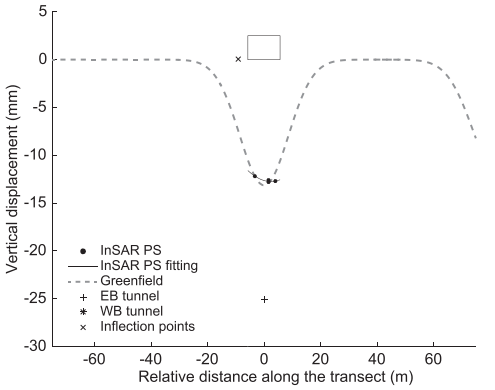

(j2) case j, transect

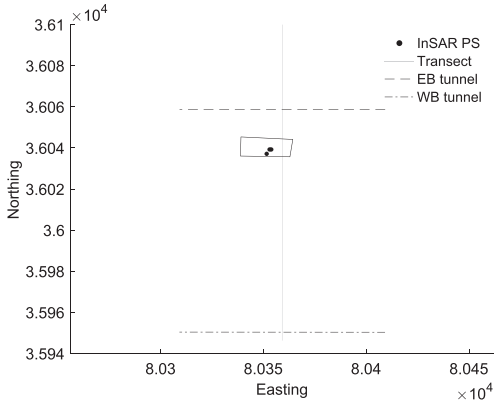

(k1) Case k, plan

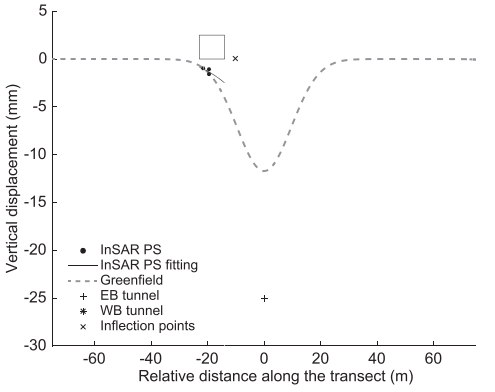

(k2) case k, transect

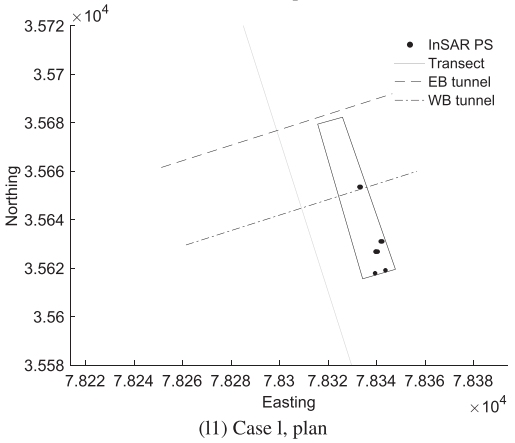

(l1) Case l, plan

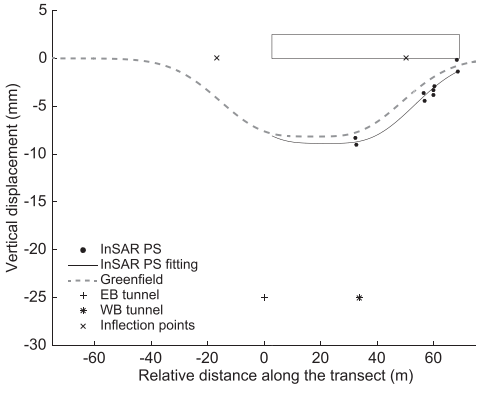

(l2) case l, transect

FIGURE A1 Continued

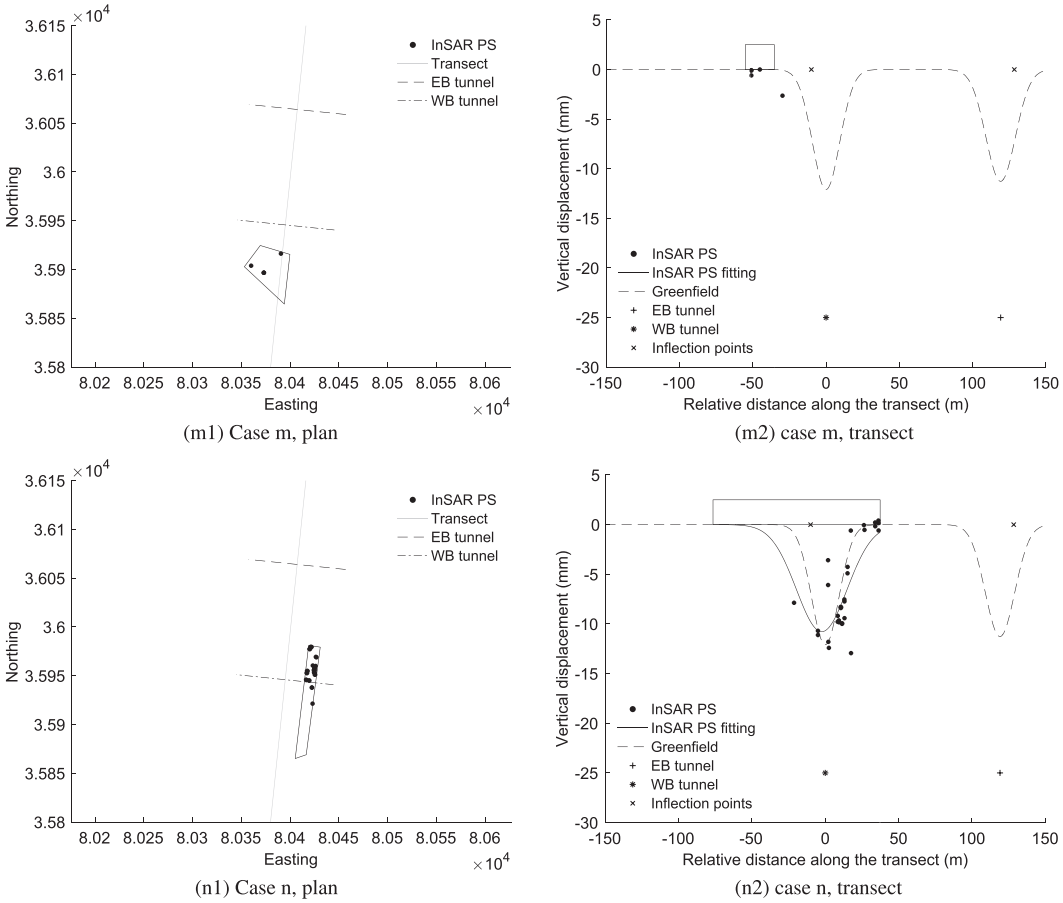

(m1) Case m, plan

(m2) case m, transect

(n1) Case n, plan

(n2) case n, transect

FIGURE A1 Continued

TABLE A1 Coefficients α, β and γ (Equation 13) of the modified Gaussian fitting curve for the buildings analysed in this study

Case	α	β	γ
a	8.8409	1.8090	1.3875
b	−5.3212	1.0000	1.0674
c	−9.9545	1.5420	1.1387
d	2.9446	1.0487	1.2738
e	−9.9668	2.4865	1.6167
f	−10.0000	1.8105	1.5159
g	−9.8997	2.0123	2.4024
h	6.9282	1.0000	1.1127
i	−8.4925	2.7793	1.8407
j	−2.4038	2.1216	2.1867
k	−9.9720	1.1215	1.6184
l	−4.2477	1.0874	1.0000
m	−10.0000	1.0000	1.0000
n	2.3999	1.6466	1.8478